IEEE Access
Multidisciplinary | Rapid Review | Open Access Journal

Date of publication xxxx 00, 0000, date of current version xxxx 00, 0000.

Digital Object Identifier 10.1109/ACCESS. 2022.Doi Number

Optimized Design of ±5 kV, 1 kA Rectangular Power Cable for a Low Pressure of 18.8 kPa for Envisioned All-Electric Wide-Body Aircraft

Anoy Saha[1], Student Member, IEEE, Mona Ghassemi[1], Senior Member, IEEE
[1]Zero Emission, Realization of Optimized Energy Systems (ZEROES) Laboratory, Department of Electrical and Computer Engineering, The University of Texas at Dallas, Richardson, TX, 75080 USA

Corresponding author: Mona Ghassemi (e-mail: mona.ghassemi@utdallas.edu)

This work was supported in part by the U.S. Advanced Research Projects Agency-Energy (ARPA-E) under Award DE-AR0001677, in part by the U.S. National Science Foundation (NSF) under Award 2306093, and in part by the U.S. Air Force Office of Scientific Research under Award FA9550-20-1-033.

ABSTRACT Power cables, one of the key components of electric power systems (EPS) in future wide-body all-electric aircraft (AEA), have a lot of room for improvement in achieving low system mass leading to high power density designs. The limited heat transfer by convection at a cruising altitude of 12.2 km (18.8 kPa) presents thermal issues for the design of aircraft power cables. The surface area of the cable influences both convective and radiative heat transfers. One way to improve radiative heat transfers and make up for the lower convective heat transfer caused by the low air pressure is to change the shape of the cable. The rectangular geometry design of cables offers a larger contact area with the surrounding atmosphere compared to cylindrical and cuboid cables of the same cross-sectional area. This paper presents the design and analysis of rectangular bipolar MVDC power cables in addition to cuboid, coaxial, and conventional cylindrical bipolar cables to determine the optimized bipolar MVDC power cable system for future wide-body AEA. To compare these designs, a parameter J is introduced that quantifies the product of the overall mass per unit length of the cables and their cross-sectional area. According to the findings, the rectangular bipolar cable systems demonstrated superior performance compared to other bipolar cable systems in terms of J and would be a solution for future wide-body AEA.

INDEX TERMS all-electric aircraft (AEA), coaxial cable, cuboid geometry, low pressure, MVDC power cables, multilayer insulation, rectangular geometry, thermal analysis.

I. INTRODUCTION

Climate change is one of the most critical issues that humanity has ever faced. Greenhouse gases (GHGs) play a major role in this by trapping heat in the atmosphere, leading to a rise in global temperatures. Transportation-related GHG emissions accounted for 28% of total U.S. GHG emissions in 2021, making it the greatest producer of U.S. GHG emissions [1]. With greater growth over the past few decades than rail, road, or shipping, aviation accounted for 2% of worldwide energy-related CO_2 emissions in 2022 [2]. Given the anticipated growth in passenger and cargo air travel, commercial aircraft emissions could triple by 2050 [3]. To solve the severe climate issue and reach the goal of net-zero emissions across all sectors by 2050, it is essential to undertake significant decarbonization activities in the transportation sector. One of the most crucial strategies for meeting the goal of net zero emissions is the electrification of transportation. Recent studies have explored the use of electrical systems in commercial aircraft as a substitute for conventional mechanical, hydraulic, and pneumatic systems to accomplish this objective [4]. Electric power systems (EPS) on upcoming generations of electrified aircraft, such as more electric aircraft (MEA) and all-electric aircraft (AEA), would need to be able to deliver a large quantity of power while reducing the total system mass. In [5], three bipolar MVDC EPS designs of ±5 kV range were proposed and analyzed for potential use in a wide-body AEA. For connecting EEUs to busbars, a maximum of 1000 A ampacity is needed. The power cables, being a key component of the EPS, offer significant potential for reducing the overall system mass through improvements. One possible strategy for reducing the weight of cables and, consequently, the total mass of the aircraft's EPS is to implement higher voltage operations [6]. However, the design

of cable insulation has major hurdles when dealing with higher voltage operation, and to date, there is no MVDC power cable built and tested for use at low pressures.

Designing cables for airplane applications involves several important considerations, such as partial discharges (PDs), surface charges, arc and arc tracking, and thermal management [7–9]. Among these, thermal management holds utmost importance due to its substantial influence on the weight, dimensions, and maximum current capacity of the cables [10]. These issues become considerably more significant in designing ±5 kV MVDC bipolar cables that operate in various environmental situations. When air pressure decreases, there is an increase in the intensity and frequency of PDs. Additionally, the partial discharge inception voltage (PDIV) decreases significantly, particularly at higher operating voltages [11]. To address these issues concurrently while preserving the goals of high-power density and low system mass, a multilayer multifunction insulation system is proposed in this paper. By utilizing numerous fluoropolymer layers inside the insulation systems and a reasonably thick fluoropolymer layer as a jacket, problems with the arc and arc tracking are solved. Surface PDs can be mitigated through the implementation of screened insulation systems in the outer regions of the insulation system.

At the cruising altitude of wide-body aircraft (12.2 km), the low air pressure of 18.8 kPa limits convective heat transfer. As a result, the maximum permissible current flowing through the cable decreases compared to atmospheric pressure [12-14]. Additionally, the use of bipolar cable systems further restricts the maximum permissible current. So, the optimal design of bipolar cable systems is crucial for achieving a high-power density and low-system-mass electrical power system (EPS) in cable aircraft applications. Increasing the radiative and convective heat transfer of the cables is one possible solution for increasing the current-carrying capacity of the cables. While an increase in surface area will result in a faster rate of radiative heat transfer, increases in convective heat transfer may be significant, minor, or even nonexistent, depending on a variety of factors, such as the shape of the cable. Cuboid (square) and rectangular cables can be utilized as a solution to make up for the decrease in the maximum permitted current at decreased pressures by increasing the outer surface area of the cable system while maintaining the same mass and cross-sectional area. To address the theoretically infinite electric field at sharp edges, it is essential to incorporate rounded corners in the design of cuboid and rectangular cables.

To the best of the authors' knowledge, there have been no investigations aimed at determining the optimal weight and dimensions for bipolar MVDC cables under low-pressure conditions. The power ratings of both screened and unscreened cables under various AC frequency and pressure conditions were investigated. Because of their higher withstand voltage and marginally improved thermal performance, screened cables offer significant advantages in aerospace applications. Some other prior studies have exclusively focused on cables not utilized in aviation. The study conducted in [15] investigated the heat dissipation of two buried cables in a trench. The study revealed a significant reduction in the maximum ampacities of cables when an additional cable is introduced into the trench. The study in [16] examined how cable spacing and the number of cables in a trench affect the ampacity of underground cables. In another study, an analytical calculation was conducted to assess the ampacity of a submarine cable with a single conductor. The analysis considered several factors that could potentially impact the cable's performance, such as ambient temperature, burial depth, and spacing distance [17].

This paper presents the design of a rectangular bipolar geometry cable with a multilayer insulation system and compares its weight and dimensions to cylindrical, cuboid, and coaxial alternatives in low-pressure conditions. For application in low-pressure situations, a rectangular bipolar MVDC power cable system with a voltage of ±5 kV has not yet been developed. The authors of [18] examined electric field characteristics surrounding insulated busbars, as well as the impact of insulation thickness and curvature under a 1 kV (peak) AC voltage. Some other authors have worked on designing rectangular wire winding for AC electrical machines. Rectangular wire windings have some advantages such as higher slot fill factor, good heat dissipation, and strong rigidity [19, 20]. Also, employing coaxial cable systems may result in a decrease in the total size, volume, and weight of the aircraft's EPSs. A coaxial bipolar cable system has a higher surface area than a standard bipolar MVDC power cable, hence radiative and convective heat exchanges are increased. To the best of the authors' knowledge, there hasn't been any research done on coaxial cable systems for use in aircraft with or without an active cooling system. The paper [21] presented a factory joining method and the design of a 120 kV coaxial integrated return conductor for submarine cable systems. A multilayer coaxial high-temperature superconducting (HTS) cable with a voltage rating of 23 kV and a power rating of 60 MVA was developed for use in a three-phase system [22]. Liquid nitrogen was employed to cool the cable. The heat dissipation performance of coaxial cable in electromagnetic launch (EML) systems was discussed in [23]. The thermal conductivity of the insulator ethylene-propylene-diene monomer (EPDM) hampers the heat dissipation capability of the coaxial cable. A high thermal conductivity material is necessary for an insulation system to enhance the temperature distribution within the insulator.

In this paper, a comprehensive finite element model (FEM) model integrating electrical, thermal, and computational fluid dynamics (CFD) has been developed to design and evaluate the most efficient bipolar cable system for a future wide-body AEA. Various bipolar cable systems, including conventional cylindrical, cuboid, rectangular, and coaxial designed with multilayer insulation systems and optimized to achieve a maximum allowable temperature of 260°C under a current of 1000 A and pole voltages of +5 kV and -5 kV, respectively. A

comparative study was conducted among those designs to determine the optimal combination of bipolar cable systems for future wide-body AEA applications.

II. MODEL

A. DESIGNING CUBOID, RECTANGULAR, AND COAXIAL BIPOLAR CABLE SYSTEMS

For aircraft applications, to develop an efficient EPS that exhibits high power density and low system mass, the cables need to be designed to either support a higher maximum current with the same cross-sectional area and mass or have a smaller cross-sectional area and mass while maintaining the same ampacity. In this paper, the second approach is considered for designing the MVDC bipolar cables. In the second approach, thermal analysis is required while designing cables to accomplish a high-power-density and low-system-mass EPS. A cable's total heat loss at its core conductor can be expressed as the sum of its radiative and convective heat transfers.

$$Q = Q_r + Q_c \tag{1}$$

where Q is the core conductor's total heat loss (W. m^{-3}), Q_c is the convective heat transfer (W.m^{-3}), and Q_r is the radiative heat transfer (W. m^{-3}). For a given ampacity, decreasing the mass and cross-sectional area of the cables will increase Q. This is because decreasing the cross-sectional area increases the resistivity of the core conductor. Hence, it is necessary to improve the radiative and convective heat transfers to make up for the increase in total heat loss.

The radiative heat transfer from the object's surface which has a uniform temperature, can be determined by

$$Q_{r_i} = \sum_{j=1}^{N} \frac{J_i - J_j}{\left(A_i F_{ij}\right)^{-1}} \tag{2}$$

where N represents the total number of objects that share radiative heat with the object i, A_i represents the surface area (m^2) of the object i, and F_{ij} represents the view factor of object j relative to the object i. Additionally, J_i and J_j represent the radiosities of objects i and j, respectively, and can be determined by solving a system of N equations:

$$\frac{E_{bi}(T) - J_i}{(1-\varepsilon_i)(\varepsilon_i A_i)^{-1}} = \sum_{j=1}^{N} \frac{J_i - J_j}{\left(A_i F_{ij}\right)^{-1}} \tag{3}$$

where ε_i represents the surface emissivity of the object i, and E_{bi} can be calculated for each object as

$$E_{bi}(T) = n^2 \sigma_S T_i^{\,4} \tag{4}$$

where n is the refractive index of air ($n \approx 1$), T_i is the i object's surface temperature (K), and σ_S is the Stefan's constant (W.m^{-2}K^{-4}).

For the cylindrical, rectangular, and cuboid bipolar cable systems, the view factor of the positive and negative poles to each other, F_{12}, and the duct to the poles, F_{13}, can be stated as

$$F_{12} = \int_{A_1} \frac{cos\theta_1 cos\theta_2}{\pi R^2} dA_1 \tag{5}$$

$$F_{13} = 1 - F_{12} \tag{6}$$

where A_1 is the surface area (m^2) of the poles, R (m) is the line that connects any two points on the surface of the poles without crossing them, θ_1 and θ_2 are the polar angles that R forms with the pole surface normals, respectively, and dA_1 is the elemental area.

Since the coaxial cable interacts only with the duct in the coaxial bipolar cable system, F_{12} equals to zero. By assuming that the poles have an equal radiosity, $J_1 = J_2$, and utilizing (4) and (6), one may further reduce (1) and obtain the radiative heat transfer of the poles as

$$Q_{r_1} = Q_{r_2} = \frac{A_1 \sigma_S (T_1^4 - T_3^4)}{\frac{1-\varepsilon_1}{\varepsilon_1} + \frac{1}{(1-F_{12})} + \frac{2(1-\varepsilon_3)}{\varepsilon_3 \left(\frac{A_3}{A_1}\right)}} \tag{7}$$

and the formula for the total radiative heat transfer is,

$$Q_r = Q_{r_1} + Q_{r_2} \tag{8}$$

Radiative heat transfer rises with increasing surface area of the poles, as shown by (7), provided that this increase is greater than the increase in the view factor between the poles, F_{12}. Increasing the surface area of cylindrical, rectangular, and cuboid configurations results in an increase in F_{12} for a given distance between the poles. When the overall diameter of the cylindrical cable is 1 inch, the outer surface area, A_1, of cuboid and rectangular cables with a given cross-sectional area is compared to the cylindrical one, resulting in:

$$A_{1_{cuboid}} = \left(\frac{2}{\sqrt{\pi}}\right) A_{1_{cylinderical}} \tag{9}$$

$$A_{1_{rectangular}} = \left(\frac{6}{\sqrt{5\pi}}\right) A_{1_{cylinderical}} \tag{10}$$

In Table I, the ratio of the view factor of poles to each other, F_{12}, at the distances of 0 to 2 inches between the poles are shown. As can be seen from (9) and (10), the surface area of the cable rises by roughly a factor of $2/\sqrt{\pi}$=1.13 and $6/\sqrt{5\pi}$=1.51, when the shape is changed from cylindrical to cuboid and cylindrical to rectangular, respectively.

TABLE I
THE RATIO OF VIEW FACTORS BETWEEN TWO POLES WITH DIFFERENT DISTANCES BETWEEN THEM

Distance between the poles	$F_{12cuboid}$ / $F_{12cylindrical}$[a]	$F_{12rectangular}$ / $F_{12cylindrical}$[a]
0	1.3760	0.4587
0.5	1.3189	0.2622
1	1.1654	0.1955
1.5	1.0586	0.1677
2	0.9878	0.1527

[a]View factors are calculated for, without rounding the edges of the cuboid and rectangular cables.

However, from Table I, it can be shown that the view factor also increases for small distances between the poles, however, by increasing the distance between the poles, its value decreases, leading to further enhancing the radiative heat transfer. Furthermore, rectangular shapes consistently exhibit a ratio of less than 1, indicating a more favorable radiation effect. Nevertheless, radiative heat transfer of a cuboid bipolar cable system at small distances may be lower than that of a cylindrical one; thus, it is important to select a material with a certain range of emissivity for the duct and cables and to optimize the size of the cables and the duct to reduce this effect.

The radiative heat transfer for the coaxial bipolar cable system is represented as

$$Q_{r_{coaxial}} = \frac{A_1 \sigma_S (T_1^4 - T_3^4)}{\frac{1-\varepsilon_1}{\varepsilon_1} + \frac{1}{F_{13}} + \frac{1-\varepsilon_3}{\varepsilon_3 \left(\frac{A_3}{A_1}\right)}} \tag{11}$$

where $F_{13} = 1$. With the surface temperature of the cable being the same as that of a cylindrical cable, the radiative heat transfer in the coaxial cable system improves. The entire radiative heat transfer for the coaxial wire, however, is calculated as

$$Q_r = Q_{r_{coaxial}} \tag{12}$$

meaning that to provide an amount of radiative heat transfer equal to a cylindrical bipolar cable system, the surface area of a coaxial bipolar cable system should be roughly double that of each pole for a cylindrical one. Radiative heat transfer is enhanced in square and rectangular cables due to their larger outer surface area compared to cylindrical cables. While square or rectangular cables may face limitations in bend radii depending on orientation, cylindrical cables generally offer greater flexibility, allowing uniform bending in all directions. Square and rectangular cables can sometimes be packed more densely than round ones, taking up less space when used in certain applications. This is especially useful in small spaces or situations where space utilization is critical.

The convective heat transfer for a cylindrical cable can be empirically expressed as

$$Q_c = \pi k (T_1 - T_3) \left(0.6 + \frac{0.387 {Ra_D}^{\frac{1}{6}}}{\left(1 + \left(\frac{0.599}{Pr}\right)^{\frac{9}{16}}\right)^{\frac{8}{27}}} \right)^2 \tag{13}$$

where k is thermal conductivity (W.(K.m)$^{-1}$) of the air, Ra_D and Pr are Reynold and Prandtl numbers that are respectively given by,

$$Ra_D = \frac{g \rho^2 C_p \alpha_p (T_s - T_{ext}) {D_{ch}}^3}{k \mu} \tag{14}$$

$$Pr = \frac{\mu C_p}{k} \tag{15}$$

where D_{ch} is the cable's characteristic diameter (m) and usually equals to the diameter of the cable, μ is the dynamic viscosity of the fluid (Pa.s), C_p is the heat capacity of the air (J.(kg.K)$^{-1}$), g is the acceleration of the gravity (m.s^{-2}), ρ is the air density (kg.m^{-2}), and α_p is the coefficient of thermal expansion (K^{-1}). The material data are evaluated at the average of T_3 and T_1 except for the air density which is calculated at T_1.

For a cuboid and rectangular shape cable, the governing equation of convective heat transfer is not as straight as (13), therefore, a comparison between the convective heat transfers is not possible by using these empirical expressions. Nevertheless, the coaxial bipolar cable system has the same cylindrical shape as the cylindrical bipolar cable system, so it can be concluded from (13)-(15) that the convective heat transfer of the coaxial bipolar cable system is larger.

Equation (13) is for one pole of the cylindrical bipolar cable system, so for the coaxial cable system to have the same convective heat transfer, the overall diameter of the coaxial cable system needs to be increased by approximately 2 times each pole. Therefore, same as the issue for the radiative heat transfer, the cross-sectional and mass of the coaxial bipolar cable system will be 2 times that of the cylindrical bipolar cable system.

B. COUPLED ELECTRICAL, THERMAL, AND CFD MODEL OF BIPOLAR CABLE SYSTEMS

Equations (1)-(13) provide insight into the analysis of design parameters that affect radiative and convective heat transfers. However, it is important to note that these equations are primarily based on specific assumptions for a given condition. Therefore, for all case studies, employing (1)–(13) offers approximative findings for comparing bipolar cable systems. To assess the electrical and thermal performance of various types of bipolar MVDC power cables used in wide-body aircraft at a typical cruising altitude of 12.2 km above sea level, an integrated model combining electrical, thermal, and CFD is developed in COMSOL Multiphysics. The model incorporates laminar flow, magnetic fields, heat transfer modules, surface-to-surface heat radiation, and electric currents modules. The modeling process considers all three forms of heat transfer: conduction, convection, and radiation. Fig. 1 describes the flowchart of the modeling procedure and Fig. 2 depicts the configuration of the multilayer insulation system considered for cables. This insulation system is used for rectangular, cuboid, and conventional bipolar cable systems studied in this paper. This design demonstrates superior performance in addressing the challenges associated with aircraft power cables operating in diverse environmental conditions. This cable design incorporates both polyamides (PI) and fluoropolymer polymers in the insulation system to achieve an optimal design that effectively prevents arcing and arc tracking, while also meeting higher breakdown voltage

requirements. It consists of a Teflon® PFA layer (0.5-mil) and a Kapton® MT+ layer (1.5-mil) enclosed in a 6.5-mil film. This design enhances the breakdown voltage within the inner portion of the insulation. The insulation also consists of a 5 mil-thick copper screen layer located between the wrapped layers and the outermost layer. The outermost layer is 4 mils thick Teflon® PFA jacket. Table II represents the characteristics of the materials used in the different shapes of bipolar cable systems.

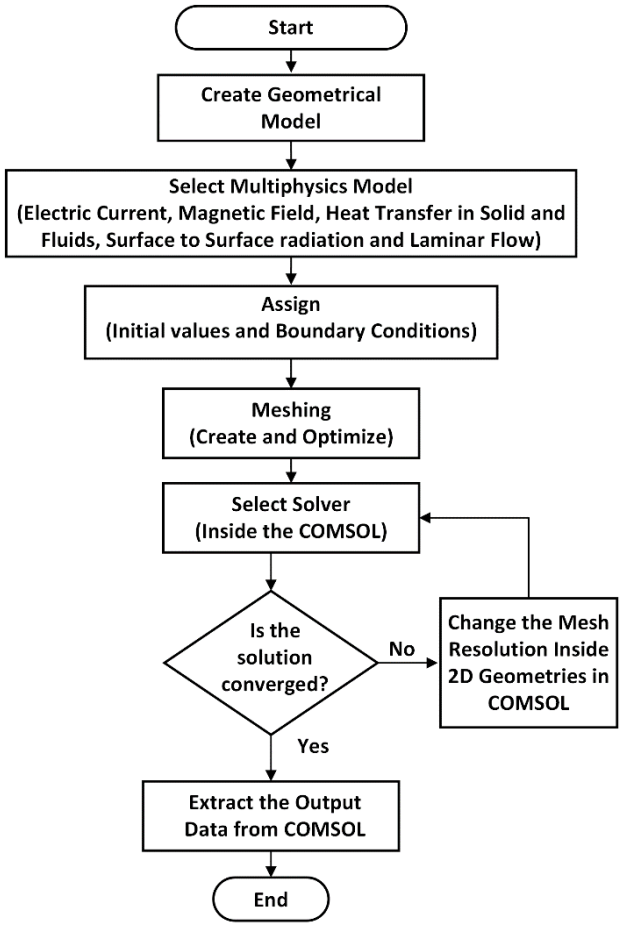

FIGURE 1. Flowchart of modelling procedure using COMSOL Multiphysics Software.

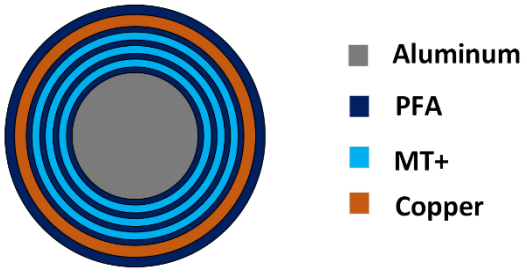

FIGURE 2. The Multilayer insulation system considered for the Cable.

TABLE II
CHARACTERISTICS OF THE MATERIAL USED IN MULTILAYER INSULATION CONFIGURATION [24, 25]

Parameters	Teflon® PFA	Kapton® MT+	Aluminum 1350	Copper
Thermal Conductivity (W.(m.K)$^{-1}$)	0.195	0.75	238	400
Dielectric Constant	2	4.2	-	-
Density (Kg.m^{-3})	2150	1420	2705	8960
Dielectric Strength (V.m^{-1})	256×10^{6}	208.5×10^{6}	-	-

Fig. 3–6 show the 2D geometries of the four types of bipolar cable systems that are utilized for modeling and simulations in this study. The multilayer insulation configuration is utilized for the main insulating system of both poles of cylindrical, cuboid, and rectangular bipolar cable systems. To simulate heat radiation, the bipolar cable system is enclosed in the duct, which is shown as the ambient surface in Figs. 3–6. The duct is a 1 mm thick square-shaped domain. The duct's side (L) measures 1 m in length. The duct's outside surface remains at a constant temperature of 40°C, and the pressure inside the duct is 18.8 kPa, representing the conditions encountered at the cruising altitude of a wide-body aircraft. The "S" in Figs. 3–6 represents the separation between the negative and positive poles. Bipolar cables for future wide-body airplanes are optimally designed regarding "S". Additionally, a sufficient gap must be kept between the cable and the duct sides to guarantee that the failure of the cable won't jeopardize the safety of the aircraft or its systems. For all the simulations utilized in this work, the poles are placed 1 inch above the duct floor as recommended in [26]. Rounded corners were utilized in cuboid (square) and rectangular geometry to reduce the infinite electric field intensity caused by sharp edges.

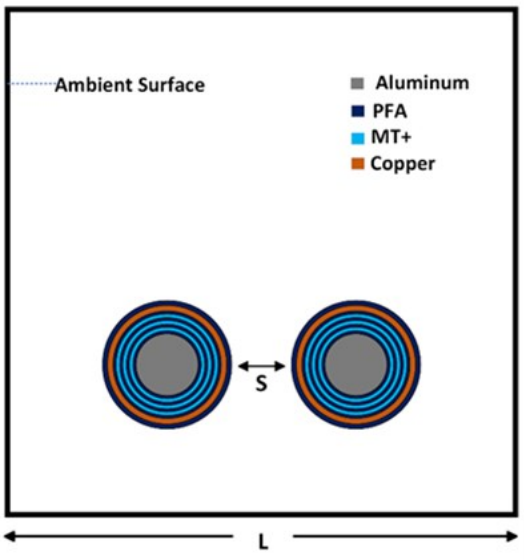

FIGURE 3. Geometries of the conventional cylindrical bipolar cable systems.

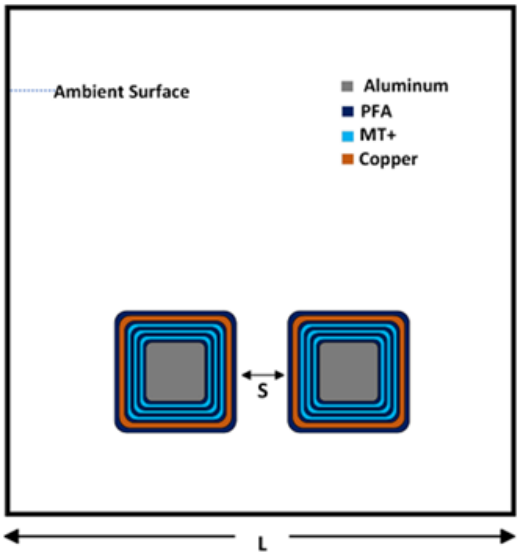

FIGURE 4. Geometries of the cuboid (square) bipolar cable systems.

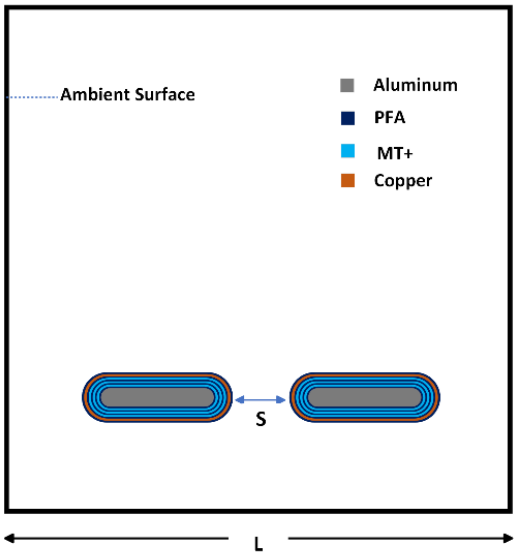

FIGURE 5. Geometries of the rectangular bipolar cable systems.

In Fig. 6, the 2D geometry of the coaxial bipolar cable system is shown. In coaxial bipolar cable systems, the cross-sectional area of the inner and outer conductors is assumed to be equal. The same 6.5-mil-thick-wrapped insulation configuration is utilized for the insulation between inner and outer conductors/poles. For the outer insulation, the same insulation layers as cylindrical cables are used. The inner conductor/pole voltage is +5 kV, while the outer conductor/pole voltage is -5 kV. For having the same cross-sectional area for the inner and outer conductors of coaxial bipolar cable systems, the following formula is used.

$$r_{con1}^2 = r_{con3}^2 - r_{con2}^2 \tag{16}$$

where r_{con1} is the radius of the outer part of the inner conductor, r_{con2} is the radius of the inner part of the outer conductor and r_{con3} is the radius of the outer part of the outer conductor.

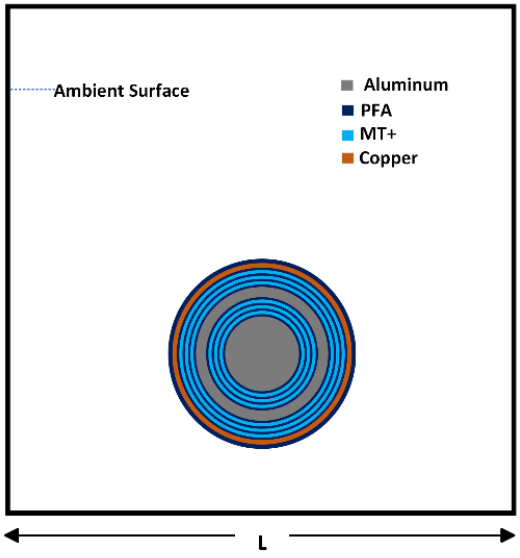

FIGURE 6. Geometries of the coaxial bipolar cable systems.

The heat equation from the cable's core conductor to its outside can be written as:

$$\rho C_p \frac{\partial T}{\partial t} + \nabla.(-k\nabla T) = Q + q_o \tag{17}$$

where ρ is the density (kg.m^{-3}), k is thermal conductivity (W.(K.m)$^{-1}$), C_P is the specific heat capacity at the constant pressure (J.(kg.K)$^{-1}$), T is the temperature (K), and q_o is the net outward radiative heat flux (W. m^{-3}). Q is the amount of heat (W.m^{-3}) that comes from joules heat loss. It can be written as:

$$Q = I^2 R \tag{18}$$

where I represents conductor current (A) and R represents the resistance (Ω).

Considering P_1 is a point located on the surface of the cable, the net outward radiative heat flux (q_o) at P_1 is expressed by:

$$q_o = \varepsilon_1 (E_{b1}(T) - G_{12}) \tag{19}$$

where ε_1 is the emissivity of the cable surface, G_{12} is the irradiation received at point P_1 from the ambient surface (W.m^{-2}), and $E_{b1}(T)$ is the power radiated across all wavelengths (W.m^{-2}) from P_1. The heat equation in the air domain can be described as:

$$\rho\rho C_p \frac{\partial T}{\partial t} + \rho C_p u.\nabla T + \nabla.(-k\nabla T)$$

$$= Q + q + \tau : \nabla u + \frac{-T}{\rho}\frac{\partial \rho}{\partial t}\left(\frac{\partial P}{\partial t} + u.\nabla P\right) \quad (20)$$

where ρ is the density of the air (kg.m^{-3}), C_p is the heat capacity at the constant pressure (J.(kg.K)$^{-1}$), u is the air velocity vector (m.s^{-1}), k is the thermal conductivity of the air (W.(K.m)$^{-1}$), T is the temperature (K), τ is the viscous tensor (Pa), q is the heat flux (W.m^{-3}) and P is the pressure (Pa). The operator ":" stands for the double dot product. The fluid (here air) velocity field can be determined from the momentum equation and the equation of continuity that are respectively described as:

$$\rho \frac{\partial u}{\partial t} + \rho(u.\nabla)u = \nabla.(-PI_I + \tau) + (\rho - \rho_{ref})g \quad (21)$$

$$\frac{\partial \rho}{\partial t} + \nabla.(\rho u) = 0 \quad (22)$$

where ρ_{ref} is the reference density (kg.m^{-3}), and g is the acceleration of gravity (m.s^{-2}).

The distribution of the electric field can be calculated using,

$$E = -\nabla V \quad (23)$$

$$J_e = \sigma E \quad (24)$$

where J_e is the current density (A.m^{-2}), V is the voltage (V), and σ is the conductivity (S.m^{-1}). In addition, the steady-state space charge density can be determined using:

$$\sigma E.\nabla\left(\frac{\varepsilon_e}{\sigma}\right) = \rho_e \quad (25)$$

where ρ_e is the space charge density, and ε_e is the permittivity.

The conductivity of polymeric DC cables can be calculated using the empirical expression of

$$\sigma(E,T) = \sigma_0 e^{\left(\frac{-a}{T} + bE\right)} \quad (26)$$

where E is the electric field (V.m^{-1}), a is the coefficient of temperature, b is the coefficient of electric field, and σ_0 is a constant associated with the polymeric material. The Electric Current module in COMSOL Multiphysics software calculates the electric field across the insulation by solving the electrical conductivity expression. This solution includes both the current and Poisson's electric fields. Hence, the electric field present in the cables is considered as the overall electric field. The electric conductivity of Teflon® PFA and Kapton® MT+ is not available, so the electric conductivity of ETFE and PI is used as a substitute for these materials, respectively. Table III presents the parameters of (26) for PI and ETFE.

TABLE III
ELECTRICAL CONDUCTIVITY PARAMETERS OF THE MATERIAL

Parameters	σ_o (S/m)	a (K)	b (mm/kV)
PI	1.677e-9	3319	0.05558
ETFE	2.027e-10	4061	0.03097

Equations (17)-(26) demonstrate the coupling between the temperature field, velocity field, and electric field. To mitigate the risk of system failure and breakdown, the insulation system for the MVDC cable system was designed based on the following criteria:

$$E_{\max(i)} < 0.8E_{bd(i)} \quad i = 1:n \quad (27)$$

where $E_{max(i)}$ and $E_{bd(i)}$ are the maximum electric field and breakdown strength of i-th dielectric layer, respectively, and n is the number of dielectric layers. To compare the bipolar cable system, a parameter of J can be defined as

$$J = m.A \quad (28)$$

where A is the overall cross-sectional area of the bipolar cable system (m^2), and m is the total cable's mass per unit length (kg.m^{-1}). Designs with a smaller J are preferred because they allow for higher power densities and lower total system masses. The computational complexity of a FEM simulation in COMSOL Multiphysics can vary depending on several factors, including the specific physics modules involved, the mesh size, the solver settings, boundary conditions and the complexity of the geometry. For reaching the steady state, the simulation time is considered 30 hours in this model.

III. SIMULATION RESULTS AND DISCUSSION

The primary goal of this study is to develop a high-power-density, low-system-mass bipolar MVDC power cable system for wide-body AEA. The core was designed using specialized high-temperature conductors, 1350-O aluminum wires with 63% IACS, which can withstand temperatures up to 260°C. For all bipolar cable systems, the overall diameter of the core conductor of the cable is determined to achieve the maximum permissible temperature of 260°C, when the current is 1000 A, the temperature of the duct is 40°C, the voltage of the poles is +5 kV and -5 kV, and the air pressure is 18.8 kPa. Using the coupled model, all bipolar cable systems are optimized and analyzed.

A. CYLINDRICAL BIPOLAR CABLE SYSTEMS

Table IV represents the data for conventional cylindrical MVDC bipolar cable systems. The data presents the distance between the cables, core conductor's minimum diameter to maintain the maximum permissible temperature of 260°C, minimum diameter of the cables, surface area of the cables, weight per unit length of the cables, and J of the cable systems proposed in section II.B. The studied geometry is depicted in Fig. 3.

TABLE IV
OPTIMIZED DATA FOR CYLINDRICAL BIPOLAR CABLE SYSTEMS

Distance between the poles (inch)	Core conductor diameter (mm)	Cable diameter (mm)	Cross-sectional area of the cable (mm^2)	Weight per unit length (kg.m^{-1})	J (g.mm)
0	19.18	19.967	626.25	1.7636	1104.46
0.5	17.97	18.757	552.65	1.5602	862.25
1	17.90	18.687	548.53	1.5488	849.56
1.5	17.81	18.597	543.26	1.5342	833.47
2	17.74	18.527	539.18	1.5320	821.17

From the chart, it can be shown that by increasing the distance between the cables, S, the core conductor diameter reduces. As a result, the cables' overall diameter as well as the surface area also decreases. Minimum J is found for S=2 inches distance between the cables, 821.17 g.mm, which is about 25% lower than the J found for S=0 inches distance, when the value is 1104.46 g.mm.

B. CUBOID BIPOLAR CABLE SYSTEMS

Table V presents the data for cuboid bipolar MVDC cable systems. The data presents the distance between the cables, core conductor's one side length, overall cables one side length, surface area of the cable, weight per unit length of the cable, and J of the cable systems described in section II.B. The studied geometry is depicted in Fig. 4.

TABLE V
OPTIMIZED DATA FOR CUBOID BIPOLAR CABLE SYSTEMS

Distance between the poles (inch)	Core conductor diameter (mm)	Cable diameter (mm)	Cross-sectional area of the cable (mm^2)	Weight per unit length ($kg.m^{-1}$)	J (g.mm)
0	17.10	17.89	633.58	1.7923	1135.57
0.5	15.86	16.65	548.62	1.5569	854.15
1	15.59	16.37	530.86	1.5076	800.32
1.5	15.52	16.31	526.83	1.4965	788.40
2	15.49	16.28	524.53	1.4901	781.60

As it can be seen from the data, the lowest weight per unit length, thus the lowest J for cuboid bipolar cable systems is found for S=2 inches distance. The overall cross-sectional area also decreases when the distance between the cables increases. Therefore, the minimum J is found for S=2 inches distance between the cables, 781.60 g.mm, which is about 31% lower than the J found for S=0 inches distance.

C. COAXIAL BIPOLAR CABLE SYSTEMS

Table VI presents the geometrical configuration and analyzed data for coaxial bipolar cable systems. The geometry of the coaxial bipolar cable systems is depicted in Fig. 6. The voltage of the inner and outer conductors are +5 kV and -5 kV, respectively and both conductors are designed for carrying the same ampacity of current, 1000 A. The coaxial bipolar cable's overall diameter is 29.052 mm and the weight per unit length of the cable is 1.8329 kgm^{-1}.

TABLE VI
OPTIMIZED DATA FOR COAXIAL BIPOLAR CABLE SYSTEMS

Parameters	Value
Diameter of the inner conductor (mm)	19.82
Diameter over insulation between inner and outer conductor (mm)	20.15
Diameter of the outer conductor (mm)	28.264
Overall diameter of the cable (mm)	29.052
Cross-sectional area of the cable (mm^2)	662.86
Weight per unit length of the cable ($kg.m^{-1}$)	1.8329
J (g.mm)	1214.956

D. RECTANGULAR BIPOLAR CABLE SYSTEMS

Table VII presents the geometrical configuration and analyzed data for rectangular bipolar cable systems. The data presents the distance between the cables, core conductor's length and width, overall cable length and width, cross-sectional area of the cable, weight per unit length of the cable, and J of the cable systems described in section II.B. The geometry of the rectangular bipolar cable systems is depicted in Fig. 5.

TABLE VII
OPTIMIZED DATA FOR RECTANGULAR BIPOLAR CABLE SYSTEMS

Distance between the cables (inch)	Core conductor length (mm)	Core conductor width (mm)	Cable total length (mm)	Cable total width (mm)	Cross sectional area of the cable (mm^2)	Weight per unit length ($kg.m^{-1}$)	J (g.mm)
0	34.37	6.87	35.16	7.66	534.45	1.5380	821.98
0.5	32.68	6.54	33.47	7.32	486.27	1.4033	682.38
1	32.38	6.48	33.17	7.26	477.89	1.3794	659.20
1.5	32.14	6.43	32.94	7.22	471.42	1.3617	641.93
2	32.05	6.41	32.84	7.20	468.97	1.3548	635.36

As it can be seen from the data, the lowest weight per unit length, thus the lowest J for rectangular bipolar cable systems is found for S = 2 inches distance. The overall cross-sectional area also decreases when the distance between the cables increases. Therefore, the minimum J is found for S = 2 inches distance between the cables, 635.36 g.mm, which is about 22.7% lower than the J found for S=0 inches distance.

E. COMPARISON BETWEEN FOUR TYPES OF BIPOLAR CABLE SYSTEMS

Figs. 7 and 8 compare the four types of bipolar cable systems in terms of weight per unit length and cross-sectional area.

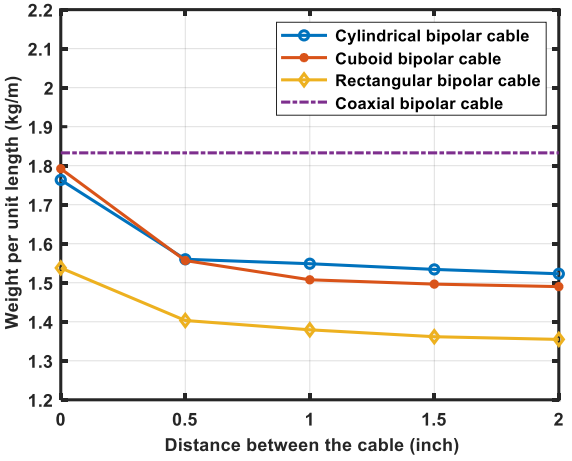

FIGURE 7. The weight per unit length of four types of bipolar cable systems.

As shown in Figs. 7 and 8, for cylindrical, cuboid, and rectangular bipolar cable systems, when the distance between the cables is 0 inches, both the weight per unit length and the cross-sectional area are higher compared to larger distances. The lowest weight per unit length and cross-

sectional area are found at 2 inches between the cables for cylindrical, cuboid, and rectangular bipolar cables. At S = 2 inches, the weight per unit length of rectangular bipolar cables is 1.3548 kg.m^{-1} which is about 9% and 11.5% smaller than the cuboid and cylindrical bipolar cables, respectively, and 26% smaller than coaxial bipolar cables. Similar types of results are also found in terms of cross-sectional area. The rectangular bipolar cables at S = 2 inches have the lowest cross-sectional area than the other cables.

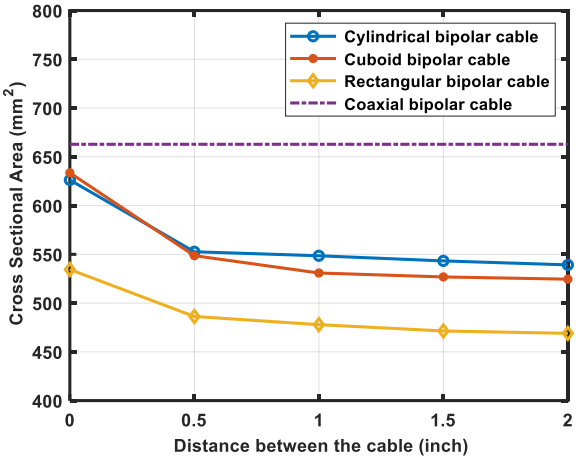

FIGURE 8. The cross-sectional area of four types of bipolar cable systems.

In Fig. 9, the parameter *J* of four types of bipolar cable systems is shown. The change in the *J* of cylindrical, cuboid, and rectangular bipolar cable systems follows a consistent pattern, with larger values observed at S = 0 inches compared to S = 2 inches. The cuboid bipolar cable system has a smaller *J* than the cylindrical one at distances of S = 0.5, 1, 1.5, and 2 inches, except at S = 0 inches but has a larger *J* than the rectangular bipolar cables at all distances between the cables. So, at a particular distance between the cables, the lowest value of *J* is found for rectangular bipolar cables. At S = 0 inches, *J* of the rectangular bipolar cable systems is 821.98, which is 25.5% and 27.61% lower than the cylindrical bipolar cable systems and cuboid bipolar systems, respectively and 32.34% lower than the coaxial bipolar cable systems. At S = 2 inches, *J* of the rectangular bipolar cable systems is 635.36, which is 22.62% and 18.7% lower than the cylindrical bipolar cable systems and cuboid bipolar systems, respectively and 47.66% lower than the coaxial bipolar cable systems.

The weight per unit length, cross-sectional area, and *J* of cylindrical, cuboid, and rectangular bipolar cable systems significantly decreases as the cable distance increases from 0 inches to 2 inches. However, as the distance between the cables is increased further, the rates of reduction tend to decrease slowly. To better understand these trends and analyze the influencing parameters, the radiative and convective heat fluxes of four types of cables are shown in Figs. 10 and 11. As the distance between the poles increases, the radiative heat flux of cylindrical, cuboid, and rectangular bipolar cable systems increases. However, higher radiative heat transfer is found for rectangular bipolar cable systems than the cuboid and cylindrical bipolar cable systems, since the changes in the view factor of the poles to each other for the rectangular cable systems is greater than cuboid and cylindrical bipolar cable systems.

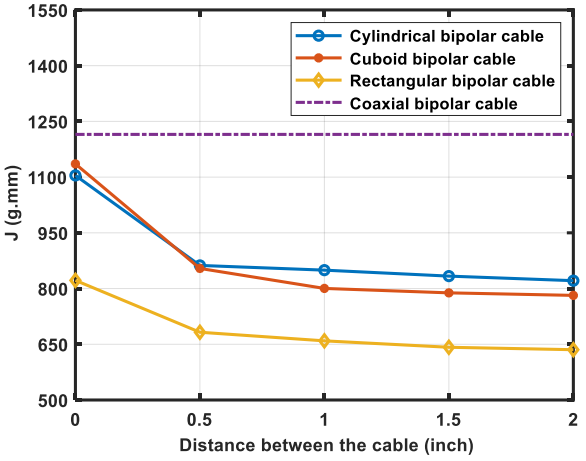

FIGURE 9. The parameter *J* of four types of bipolar cable systems.

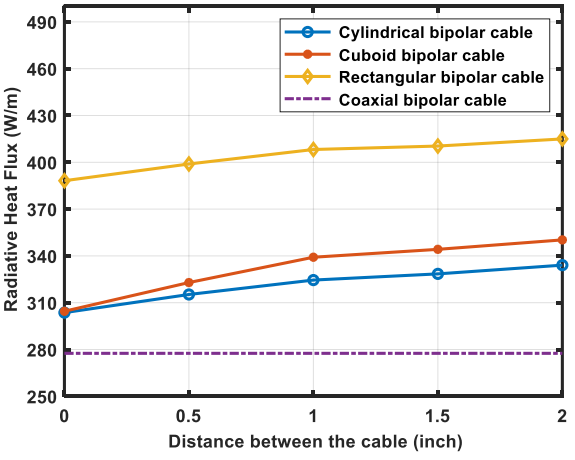

FIGURE 10. The radiative heat transfer of four types of bipolar cable systems.

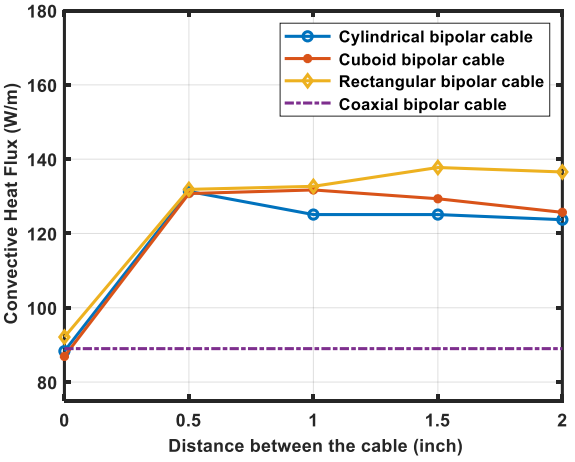

FIGURE 11. The convective heat transfer of four types of bipolar cable systems.

At S = 0 inches distance between the cables, the radiative heat fluxes of cuboid and cylindrical bipolar cable systems are almost similar and that is about 304 W.m^{-1}, however, these values are about 9.5% larger than the radiative heat fluxes of coaxial cables and about 21.7% smaller than the rectangular bipolar cables. As the distance increases, the cross-sectional area of rectangular bipolar cables is smaller than that of cuboid and cylindrical bipolar cables, Fig. 8. Despite decreasing the cross-sectional area of rectangular cables, the radiative heat transfer increases as the distance between the cables increases. This is because of the varying view factor of the poles to each other of rectangular bipolar cables, which compensates for the deceased surface area rate, and produces a larger radiative heat transfer for the system at larger distances. At S = 2 inches, the radiative heat fluxes of rectangular bipolar cables are 414.97 W.m^{-1}, which is about 18.5% and 24.2% larger than the cuboid and cylindrical bipolar cable systems, respectively.

Fig. 10 shows the convective heat fluxes of four types of cable systems. At S = 0 inches, the convective heat fluxes of cylindrical, cuboid, and rectangular bipolar cables are much smaller than the other distances. As the cables touch each other, the lack of convection on one side drastically reduces the convective heat transfer for cylindrical, cuboid, and rectangular bipolar cable systems. The lowest convective heat transfer is found for cuboid bipolar systems at this distance, however for cylindrical, coaxial, and rectangular bipolar cable systems, the value is not so much larger. The convective heat transfer of bipolar cable systems significantly increases as the distance between the poles is increased from 0 inches. This is because larger distances allow for convective heat transfer on all sides of the cables. For cylindrical and cuboid bipolar cable systems, as the distance increases from S = 0.5 inches, the convective heat transfer reduces slightly since the cross-sectional area decreases, Fig. 8. But for rectangular bipolar, the trends are not exactly similar. The maximum convective heat transfer is found at S = 1.5 inches, for rectangular bipolar cables.

A decrease in the cross-sectional area of the conductor leads to an increase in resistance per unit length, resulting in greater heat losses for a given current. The total heat transfer, which includes both radiative and convective components, must be equal to the heat losses. For rectangular bipolar cable systems, as the cross-sectional area is lower than other bipolar cable systems, the total heat losses are greater, so it reflects in higher convective heat transfer. At S =2 inches, the convective heat flux of rectangular bipolar cables is about 136.56 W.m^{-1}, which is 8.6% and 10.38% higher than the cuboid and cylindrical bipolar cable systems, respectively.

Fig. 12 displays the magnitude of the electric field across the insulation of the bipolar cable systems. The electric field norm in cylindrical, cuboid, and rectangular bipolar cable systems is the same because the insulation thickness and potential difference across the insulation are equal. But in contrast to other bipolar cable systems, the coaxial cable system's insulation has a greater potential difference, 10 kV, which raises the electric field norm throughout the insulation.

Equations (23)–(25) can be used to determine the distribution of the electric field across the insulation of DC cable systems. The electric field distribution in DC cable systems is influenced by both conductivity and permittivity.

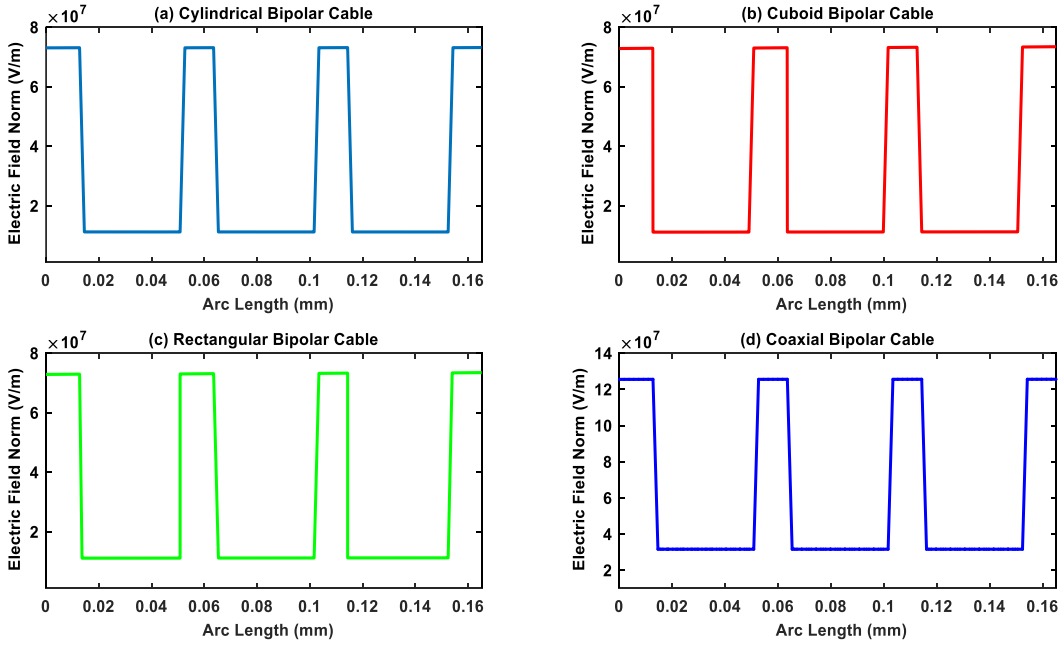

FIGURE 12. The Electric Field Norm of four types of cable systems: (a) Cylindrical bipolar cable systems; (b) Cuboid bipolar cable systems; (c) Rectangular bipolar cable systems; and (d) Coaxial bipolar cable systems.

As a result, the ratio of electric field intensity for the insulating layers in bipolar cable systems does not just match the ratio of the permittivity of the layer. All bipolar cable systems are electrically safe to operate in a steady state when taking (27) into account.

IV. CONCLUSIONS

This paper presents a detailed analysis of bipolar MVDC power cable systems for future wide-body AEA's EPS, focusing on high-power density and low-system-mass requirements. Four types of bipolar cable systems are considered: cylindrical, cuboid, rectangular, and coaxial. Multilayer insulation systems are used to address challenges in aviation cables, such as arc tracking, PDs, and thermal management. A coupled thermal, electric, and fluid flow dynamic model is developed to conduct thermal and electrical analyses of the proposed cable systems. To assess the viability of the suggested cable systems, a parameter J is introduced, which is calculated by multiplying the weight per unit of the cables by their cross-sectional area. The rectangular bipolar cable system exhibited superior performance compared to cylindrical, cuboid, and coaxial systems in terms of J, irrespective of the distance between the poles. At S = 2 inches, the J values of the rectangular bipolar cable systems are 22.62%, 18.7%, and 47.66% lower than those of the cylinder bipolar systems, cuboid bipolar systems, and coaxial bipolar cable systems, respectively. Also, the analysis of the electric field norm across bipolar cable insulation reveals that all designed systems are electrically safe in steady-state conditions. This paper focuses specifically on the natural heat convection within the cable duct. Analyzing the impact of forced convection using varying air velocities on temperature distribution in various bipolar cable system shapes and evaluating the outcomes with natural convection in the duct could be an additional interesting area for research.

REFERENCES

[1] "Sources of greenhouse gas emissions | US EPA," *US EPA*. Accessed: Nov. 16, 2023. [Online]. Available: https://www.epa.gov/ghgemissions/sources-greenhouse-gas-emissions#transportation.
[2] "Aviation - IEA," *IEA*. Accessed: Oct. 6, 2023. [Online]. Available: https://www.iea.org/energy-system/transport/aviation.
[3] "Issue brief | The growth in greenhouse gas emissions from commercial aviation (2019, revised 2022) | White papers | EESI." [Online]. Available: https://www.eesi.org/papers/view/fact-sheet-the-growth-in-greenhouse-gas-emissions-from-commercial-aviation.
[4] H. Schefer, L. Fauth, T. H. Kopp, R. Mallwitz, J. Friebe, M. Kurrat, "Discussion on electric power supply systems for all electric aircraft," *IEEE Access*, vol. 8, pp. 84188–84216, 2020.
[5] M. Ghassemi, A. Barzkar, and M. Saghafi, "All-electric NASA N3-X aircraft electric power systems," *IEEE Trans. Transp. Electrific.*, vol. 8, no. 4, pp. 4091–4104, 2022.
[6] P. Thalin, *Fundamentals of Electric Aircraft*, SAE International: Warrendale, Pennsylvania, USA, 2019.
[7] M. Borghei and Ghassemi, "A finite element analysis model for partial discharges in silicone gel under a high slew rate, high-frequency square wave voltage in low-pressure conditions," *Energies*, vol. 13, p. 2152, 2020.
[8] M. Borghei and M. Ghassemi, "Investigation of low-pressure condition impact on partial discharge in micro-voids using finite-element analysis," in *Proc. IEEE Energy Convers. Congress & Expo. (ECCE)*, pp. 3293–3298, 2020.
[9] M. Borghei and M. Ghassemi, "Separation and classification of corona discharges under low pressures based on deep learning method," *IEEE Trans. Dielectr. Electr. Insul.*, vol. 29, no. 1, pp. 319–326, Feb. 2022.
[10] G. J. Anders, *Rating of Electric Power Cables in Unfavorable Thermal Environment*; Wiley-IEEE Press, 2005.
[11] J. Jiang *et al.*, "Partial discharge investigation under low air pressure and variable frequency for more-electric-aircraft," *IEEE Trans. Dielectr. Electr. Insul.*, vol. 28, no. 5, pp. 1793–1801, 2021.
[12] A. Saha, A. Azizi, and M. Ghassemi, "Optimal bipolar MVDC power cable designs for future wide-body all electric aircraft," *IEEE Trans. Dielectr. Electr. Insul.*, Early Access, doi: 10.1109/TDEI.2024.3355033
[13] A. Azizi, M. Ghassemi, and J. M. Lehr, "Heat transfer challenges for MVDC power cables used in wide body all electric aircraft under low pressures," *IEEE Access*, vol. 10, pp. 111811–111819, 2022.
[14] A. Saha, A. Azizi, and M. Ghassemi, "An optimal bipolar MVDC coaxial power cable design for envisaged all electric wide body aircraft," in *Proc. IEEE Conf. Electrical Insul. and Dielectr. Phenomena (CEIDP)*, 2023, pp. 1–4.
[15] M. A. Hanna, A. Y. Chikhani, and M. M. A. Salama, "Thermal analysis of power cables in multi-layered soil, I. Theoretical model," *IEEE Trans. Power Del.* vol. 8, no. 3, pp. 761–771, 1993.
[16] Y. Wang, R. Chen, J. Li, S. Grzybowski, and T. Jiang, "Analysis of influential factors on the underground cable ampacity," in *IEEE Elect. Insul. Conf. (EIC)*, Annapolis, MD, USA, pp. 430–433, 2011.
[17] R. Mardiana, "Parameters affecting the ampacity of HVDC submarine power cables," in *Proc. Int. Conf. Elect. Power Energy Conver, Syst. (EPECS)*, Sharjah, UAE, pp. 1–6, 2011.
[18] R. Lowndes and I. Cotton, "Forecasting the partial discharge inception voltage (PDIV) of insulated busbars for future aircraft power distribution systems," in *Proc. IEEE Elect. Insul. Conf. (EIC)*, 2021, pp. 189–192.
[19] Y. Zhao, D. Li, T. Pei, and R. Qu, "Overview of the rectangular wire windings ac electrical machine," *CES Trans. Elect. Machines Syst.*, vol. 3, no. 2, pp. 160–169, Jun. 2019.
[20] T. Ishigami, Y. Tanaka, and H. Homma, "Motor stator with thick rectangular wire lap winding for HEVs," *IEEE Trans. Industry Appl.*, vol. 51, no. 4, pp. 2917–2923, July-Aug. 2015.
[21] T. Yamanaka, T. Kimura, Y. Murata, and S. Odajima, "Development of coaxial integrated return conductor DC extruded insulation cable and factory joint," in *Proc. IEEE/PES Transmiss. Distribution Conf. & Exhib.*, 2002, pp. 1284–1289.
[22] S. Lee and C. Y. Hyung, "Recent progress and design of three-phase coaxial HTS power cable in Korea," *IEEE Trans. Appl. Supercond.*, vol. 29, no. 5, 1–5, 2019.
[23] F. Ma and B. Li, "Heat dissipation performance of coaxial cable for electromagnetic launch," *IEEE Trans. Plasma Sci.*, vol. 50, no. 4, pp. 1056–1064, 2022.
[24] DuPont™ Kapton® MT+, [Online]. Available: https://materials-direct.com/wp-content/uploads/2021/05/K-MT-Eng-2019.pdf.
[25] DuPont™ Teflon® PFA, [Online]. Available: https://catalog.cshyde.com/Asset/Data%20Sheet%2023-__PFA%20DuPont%20PFA%20Film%20Data%20Sheet.pdf.
[26] "AC 25.1701-1 - Certification of electrical wiring interconnection systems on transport category airplanes," 31-Oct-2022. Accessed: Jul. 28, 2023. [Online]. Available: https://www.faa.gov/regulations_policies/advisory_circulars/index.cfm/go/document.information/documentid/73476.

ANOY SAHA (Graduate Student Member, IEEE) received his B.Sc. degree from the Chittagong University of Engineering & Technology (CUET), Bangladesh. Currently, he is pursuing a Ph.D. in electrical engineering at The University of Texas at Dallas, TX, USA.

His primary research focuses on electric aircraft insulation, high voltage engineering, and dielectrics and electrical insulation.

MONA GHASSEMI (Senior Member, IEEE) received her Ph.D. degree with the first honor in electrical engineering from the University of Tehran, Tehran in 2012.

From 2013 to 2015, she was a Postdoctoral Fellow with the NSERC/ Hydro-Quebec/UQAC Industrial Chair on Atmospheric Icing of Power Network Equipment (CIGELE), University of Québec at Chicoutimi (UQAC), Chicoutimi, QC, Canada. She was also a Postdoctoral Fellow with the University of Connecticut, Storrs, CT, USA, from 2015 to 2017. In 2017, she joined the Bradley Department of Electrical and Computer Engineering, Virginia Tech, Blacksburg, VA, USA, as an Assistant Professor. In 2021, she was named both the Steven O. Lane Junior Faculty Fellow and the College of Engineering Faculty Fellow at Virginia Tech. In 2022, she joined the Department of Electrical and Computer Engineering at The University of Texas at Dallas as an Associate Professor with tenure (early tenure) and Chairholder of the Texas Instruments Early Career Award (2022–2028). She has been a Registered Professional Engineer since 2015. She has authored more than 130 peer-reviewed journal and conference papers and one book chapter. Her research interests include electrical insulation materials and systems, high voltage/field engineering and technology, power systems, and plasma science.

Dr. Ghassemi has been elected as Vice-President (Technical) of the IEEE Dielectrics and Electrical Insulation Society (DEIS) for 2024. She is also an At-Large Member of the Administrative Committee of the IEEE DEIS, a DEIS Representative in the IEEE USA Public Policy Committee on Transportation and Aerospace Policy (CTAP) and in the USA Technology Policy Council R&D Policy Committee, a Corresponding Member of the IEEE Conference Publication Committee (CPC) of the IEEE Power & Energy Society (PES), an Active Member of several CIGRE working groups and the IEEE Task Forces, DEIS Technical Committee member on Dielectrics and Electrical Insulation for Transportation Electrification, and a member of the Education Committee of the IEEE DEIS and PES. She was a member of the Nominations and Appointments Committee of IEEE DEIS. She received three most prestigious, most competitive career awards which are the 2021 Department of Energy (DOE) Early Career Research Program Award, the 2020 National Science Foundation (NSF) CAREER Award, and the 2020 Air Force Office of Scientific Research (AFOSR) Young Investigator Research Program (YIP) Award. She received the 2020 Contribution Award from the IET High Voltage Journal and also received four best paper awards. She is an Associate Editor of IEEE Transactions on Dielectrics and Electrical Insulations, IEEE Transactions on Industry Applications, IET High Voltage, International Journal of Electrical Engineering Education, and Power Electronic Devices and Components, and a Guest Editor of *Aerospace*. She was a Guest Editor of *Energies*.